Journal of Alloys and Compounds 504S (2010) S86–S90

Contents lists available at ScienceDirect

Journal of Alloys and Compounds

journal homepage: www.elsevier.com/locate/jallcom

Unusual plastic deformability in a Zr-based bulk metallic glass after structural relaxation

S.H. Xie [a], X.R. Zeng [b,c,*], H.X. Qian [b,c], Q. Hu [a], Z.Y. Zheng [b,c]

[a] School of Materials Science and Engineering, Northwestern Polytechnical University, Xi'an 710072, China
[b] College of Materials Science and Engineering, Shenzhen University, Shenzhen, China
[c] Shenzhen Key Laboratory of Special Functional Materials, Shenzhen 518060, China

ARTICLE INFO

Article history:
Received 29 June 2009
Received in revised form 26 March 2010
Accepted 2 April 2010
Available online 10 April 2010

Keywords:
Bulk metallic glass
Plastic deformation
Apparent activation volume
Structural relaxation

ABSTRACT

The structural stability is an essential problem for engineering application of bulk metallic glasses (BMGs). Constant-heating dilatometric measurements were conducted for 2 mm $Zr_{63.78}Cu_{14.72}Ni_{10}Al_{10}Nb_{1.5}$ BMG rods and two visible structural relaxation processes below T_g were found, which correspond to the obvious annihilation of free volume (FV) and the continuous decrease in coefficient of linear thermal expansion (α). After annealing the BMGs near the temperature of the main structural relaxation processes and T_g for 3600 s, the BMG rods have much FV relaxed, but still remain the amorphous structure. The microhardness of the annealed samples increases with increasing the annealing temperature, but the plastic strains remain unchanged considering the uncertainty of uniaxial compression after annealing the BMGs at the temperature below T_g. The excellent plasticity of the BMGs experienced the structural relaxation is absolutely different from those previous results of embrittlement after structural relaxation below T_g. The mechanisms of this unusual plastic deformability for the BMGs experienced the structural relaxation below T_g is discussed in the light of apparent activation volume.

1. Introduction

In the past three decades bulk metallic glasses (BMGs) have attracted considerable attention and wide investigation due to their excellent mechanical properties and potential engineering applications [1–4]. BMGs are in a metastable state and can transform to the more stable crystalline counterparts at the conditions of external applied energy, for example: isochronal or isothermal annealing [5]. The structural changes should result in the changes in BMGs' mechanical performance. For this reason it is necessary to explore the structural stability and the mechanical performance of BMGs after they suffer the processes of heating. Generally, the plastic deformation in BMGs is highly localized into a few shear bands at the ambient temperature, thus the main cracks occur. This results in a limited plastic strain (less than 2%) and catastrophic failure [7,8]. Recently, some researchers have found that the introduction of the interior or exterior heterogeneity into BMGs can largely improve the plasticity of BMGs at the room temperature. Sometimes, the heterogeneity, such as nano-crystalline or nano-quasicrystalline, phase separation, deforming-induced crystallization and micrometer-sized ductile phases, is adopted as effective heterogeneous sources to improve the plasticity of BMGs [9–19]. The large compression strain of BMGs is achieved, and even the superplasiticity occurs at the condition of a particular nanometer-sized non-homogeneous structure [20]. However, whether such heterogeneity can still exist or be effective after such BMGs suffer the structural relaxation is in question. Comparing with corresponding crystalline counterparts, the BMGs usually contain a certain amount of excess FV during quenching. Previous research findings show that FV in the glassy structure can act as the beneficial sites to initiate and bifurcate the shear bands, thus result in the good plasticity in BMGs [16,21,22]. On the other hand, the excess FV is also in a metastable state and can be annihilated at the elevated temperature, which is called structural relaxation [23–26]. As reported by previous researchers, the plasticity of BMGs always deteriorates along with the annihilation of FV upon annealing the BMGs below T_g [5,6,20]. However, the plasticity of BMGs is enhanced when they sustain warm deformation at supercooled liquid region (SLR) due to the creation of new FV upon deformation [27]. The shear bands in the deformed BMGs are believed to occur through atoms' diffusion and migration that are favored by the easy atomic mobility. Whether the amount of FV definitely influences the atomic mobility and the number of shear bands, which reflects the plasticity of BMGs, needs further exploration.

In this paper, $Zr_{63.78}Cu_{14.72}Ni_{10}Al_{10}Nb_{1.5}$ alloys are selected because they contain a large amount of FV and exhibit good plas-

* Corresponding author at: College of Materials Science and Engineering, Shenzhen University, Shenzhen 518060, China. Tel.: +86 755 26557459; fax: +86 755 26534457.
E-mail address: zengxierong@163.com (X.R. Zeng).

0925-8388/$ – see front matter © 2010 Elsevier B.V. All rights reserved.
doi:10.1016/j.jallcom.2010.04.012

ticity at room temperature [28]. Constant-heating dilatometric measurements were conducted for BMGs' rods (2 mm in diameter and 25 mm in length) and two visible structural relaxation processes with the onset temperature of 466 K and 599 K were found, which correspond to the continuous decrease in the coefficient of linear thermal expansion (α) and the obvious annihilation of FV. Annealing the BMGs at the temperature before the two visible structural relaxation processes or near T_g would result in the different FV annihilation. Studying the influence of the annealing temperature and FV changes on the plastic deformation of BMGs will be helpful to confirm the structural stability of BMGs and to understand the effectivity and mechanisms of FV in initiating the shear bands.

2. Experimental details

The $Zr_{63.78}Cu_{14.72}Ni_{10}Al_{10}Nb_{1.5}$ master alloys were prepared by arc melting mixtures of the pure elements (>99.9%) with the appropriate portions of Zr, Cu, Ni, Al and the Zr–Nb intermediate alloy that was arc-melted in advance in the Ti-gettered argon atmosphere with 99.999% purity. The alloys were remelted four times to ensure the compositional homogeneity. Finally, the cylindrical rods of 2 mm in diameter were cast by injecting the alloy melt of 1233 K into a copper mold under the argon atmosphere with 99.999% purity. The phase structures were investigated by X-ray diffraction (XRD) using a Bruker D8 Advance 18 kW X-ray diffractometer with Cu Kα radiation ($\lambda = 0.154178$ nm). The glass transition and the crystallization behavior were determined by the differential scanning calorimetry (DSC) using a TA Q200 under a continuous argon flow at the heating rate of 0.33 K s^{-1}. The dilatometric measurements were conducted on a NETZSCH DIL 402C dilatometer with a resolution of $\Delta L = 1.25$ nm at the heating rate of 0.083 K s^{-1} under a compressive load of 0.3 N. The samples for dilatometric measurements are cylindrical rods with 2 mm in diameter and 25 mm in length. The microhardness measurements were performed using a Vickers hardness tester (HXD-1000TM/LCD) with 1.961 N loading and 10 s duration on a polished surface. The quasi-static-compression tests were carried out on the cylindrical rods (2 mm in diameter and 4 mm in length) sandwiched between two tungsten carbide disks using a universal testing machine (Regr5500 Reger, China) with a initial strain rate of 5×10^{-5} s^{-1} at room temperature. Both microhardness and compression tests were repeated five times to ensure the result reliability. The samples for the compression tests were cut from the long rods. The ends of the samples were polished to make them parallel to each other and perpendicular to the axis of the rod prior to compression tests using a carefully designed jig. The stress and the strain quantities presented here are the engineering stress and engineering strain data. The morphology of the fracture and side surfaces of the fractured samples was observed by the scanning electron microscope (HITACHI S-4700).

3. Results and discussion

Fig. 1 shows the XRD patterns of the samples as-cast and annealed for 3600 s at 473 K, 613 K, 638 K and 653 K, respectively. The patterns for the annealed samples exhibit the same broad maximum, characteristic of the glassy structure, as the one for the as-cast sample, showing no detectable crystallization in the annealed samples. The DSC traces of the as-cast and annealed ZrCuNiAlNb alloy rods all exhibit an endothermic event, characteristic of the glass transition and a supercooled liquid region, followed by two exothermic events, characteristic of a sequence of crystallization, as shown in Fig. 2. The XRD and DSC results show the glassy nature of all the samples. The T_g increases with increasing the isothermal annealing temperature and gains an increment of 13.3 K after the samples were annealed at 653 K.

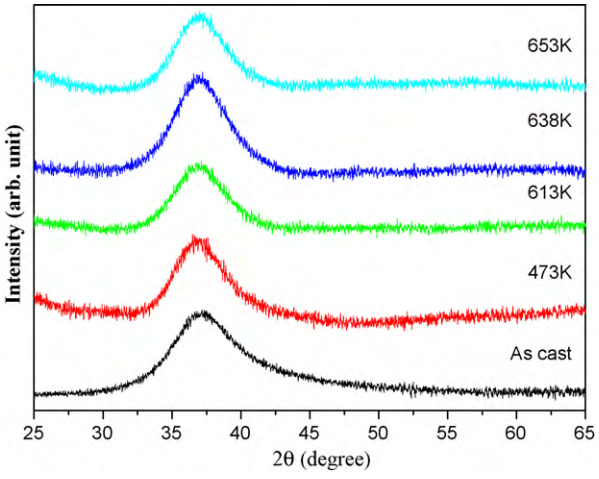

Fig. 1. X-ray diffraction patterns of the $Zr_{63.78}Cu_{14.72}Ni_{10}Al_{10}Nb_{1.5}$ alloys as-cast and annealed for 3600 s at 473 K, 613 K, 638 K and 653 K, respectively.

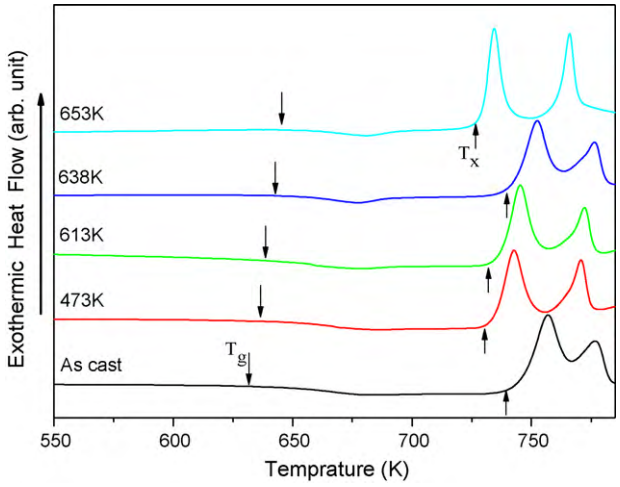

Fig. 2. DSC traces (heating rate of 0.333 K s^{-1}) of the $Zr_{63.78}Cu_{14.72}Ni_{10}Al_{10}Nb_{1.5}$ alloys as-cast and annealed for 3600 s at 473 K, 613 K, 638 K and 653 K, respectively.

Fig. 3 shows the linear thermal expansion and physical thermal expansion coefficient (α) dependence of temperature at a heating rate of 0.0833 K s^{-1}. The 1st heating cycle was up to 643 K, just below the glass transition temperature, then holding for 3600 s in order that the samples sustained the sufficient structural relaxation. The 2nd heating cycle was up to 873 K, higher than the crystallization temperature. The results show that the rod attains much relaxed excess free volume (REFV) up to 0.45% after annealing just below T_g (as indicated by a double-head arrow in Fig. 3), indicating an abundant FV content in as-cast BMGs [28,29]. The α curve of the 1st heating cycle is quite different from the one of the 2nd. At the 1st heating cycle, the alloy rod contains abundant FV and experiences the structural relaxation during heating, corresponding to the shrinkage of volume and the decrease of α. It is found that the

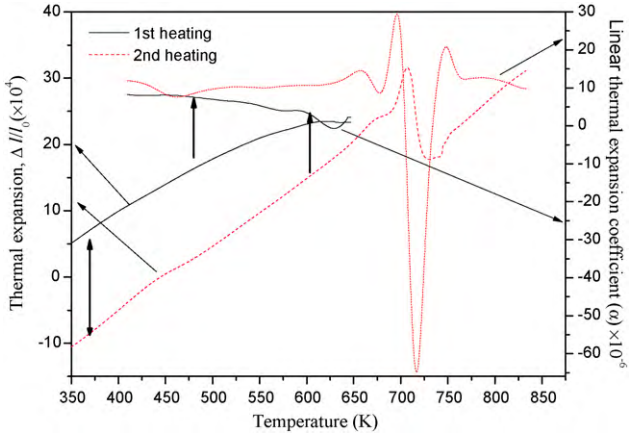

Fig. 3. The linear thermal expansion and physical thermal expansion coefficient (α) dependence of temperature for the $Zr_{63.78}Cu_{14.72}Ni_{10}Al_{10}Nb_{1.5}$ BMGs at heating rate of 0.0833 K s^{-1}. The 1st heating cycle was up to 643 K, just below the glass transition temperature, then holding for 3600 s. The 2nd heating cycle was up to 873 K, higher than the crystallization temperature.

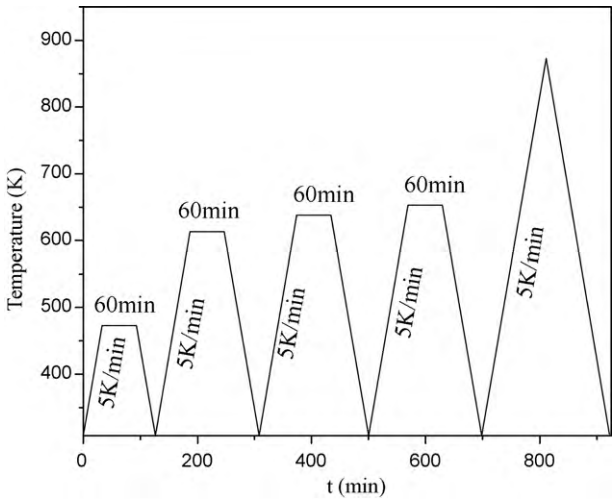

Fig. 4. The illustration of the heating cycle procedure for the loop thermal expansion experiment.

ZrCuNiAlNb BMGs go through two visible shrinkage processes at the onset temperature of 466 K and 599 K, respectively, with α value decreasing from $8.1 \times 10^{-6}\,K^{-1}$ to $-0.68 \times 10^{-6}\,K^{-1}$, corresponding to the main structural relaxation processes. However, the α value for the 2nd heating cycle below T_g remains constant due to the prior sufficient structural relaxation (about $10.3 \times 10^{-6}\,K^{-1}$). It should be noted that the fluctuation of thermal expansion coefficient at around 450 K in the 2nd heating circle is due to the non-linear relationship between the samples' temperature and time at the initial stage of heating caused the lag between the samples' temperature and the furnace' temperature by the non-contact temperature measurement in thermal dilatometer. It is reasonable to conclude that the structural relaxation begins mainly at 466 K and 599 K. To confirm this, a loop thermal expansion experiment (the details are illustrated in Fig. 4) was conducted and the results are shown in Fig. 5. In order to show the minute difference clearly, Fig. 5 is zoomed in just above the room temperature range (the inset shows the whole loop thermal expansion curves). The experiment aims to study the extent of FV annihilation by annealing the BMGs near the temperature of the main structural relaxation processes and T_g, so

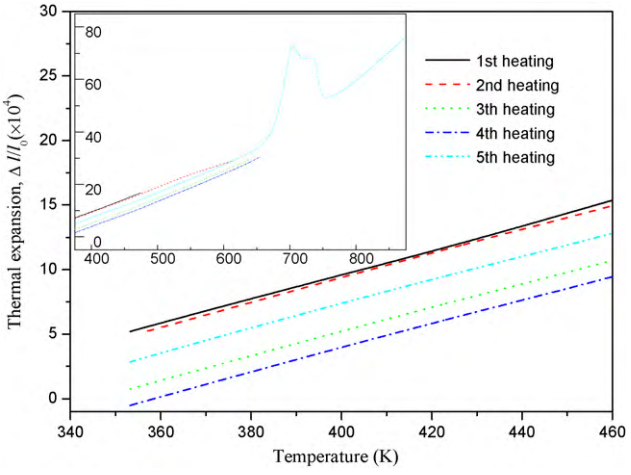

Fig. 5. The enlarged loop thermal expansion curves of the $Zr_{63.78}Cu_{14.72}Ni_{10}Al_{10}Nb_{1.5}$ BMGs just above the room temperature range. For each cycle, the rod was heated up to the fixed temperature (473 K, 613 K, 638 K and 653 K), and hold for 3600 s, then it was cooled down (the holding zones are not visible here due to the temperature reference axis). At last it was heated up to 923 K. The inset shows the whole loop thermal expansion curves.

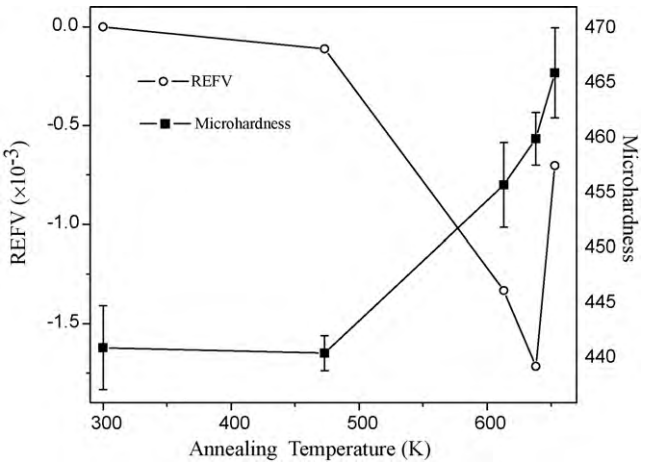

Fig. 6. The relationships of REFV and the microhardness with the annealing temperature for the $Zr_{63.78}Cu_{14.72}Ni_{10}Al_{10}Nb_{1.5}$ BMGs. The as-cast samples can be deemed as annealing at 300 K.

473 K, 613 K (just below the onset temperature of two main structural relaxation processes), 638 K and 653 K (around T_g) are selected as the isothermal annealing temperature. For the convenience of checking the REFV, the rod was cooled down to the ambient temperature after each isothermal annealing. It is shown in Fig. 6 that the excess FV is relaxed by 0.011%, 0.122% and 0.038% at the 473 K, 613 K and 638 K holding processes, respectively, indicating that more than 70% of the REFV occurs at the 2nd main relaxation temperature (599 K). It is worthy to note that the volume of the rod increases by 0.101% after annealing it just above T_g (653 K), indicating a dramatic expansion caused by the glass transition (see Fig. 6), which prevails over the shrinkage upon the structural relaxation. Because the mechanisms of glass transition are still elusive, it is difficult to essentially compare the difference between the volume changes caused by the structural relaxation and that caused by the glass transition. Whether the opposite dimensional change can cause the opposite mechanical impacts on BMGs will be discussed in the next section. The results of the microhardness testing indicate an opposite dependence of REFV at the annealing temperature below T_g (see Fig. 6). The sample annealed at 473 K exhibits just the same hardness as the as-cast one; however, the samples attain the increasing microhardness with increasing the annealing temperature. The hardness variation with the annealing temperature can be explained as following: the annihilation of FV reduces the atomic mobility and increases the whole flow stress, therefore, results in a more difficult deformation and higher hardness value. As to the sample annealed just above T_g, the microhardness still increases in spite of the dilatation upon the glass transition, which indicates there is the intrinsically difference between the dimensional change caused by excess FV and that caused by the glass transition.

In order to compare the difference in mechanical properties of BMGs with different FV content, the rods for uniaxial compression tests sustain the same annealing processes as those in dilatometric measurements. Fig. 7 shows the stress–strain curves of the as-cast and annealed $Zr_{63.78}Cu_{14.72}Ni_{10}Al_{10}Nb_{1.5}$ BMGs rods. The stress–strain curves shown in Fig. 7 represent the ones that exhibit the largest plastic strains of all five ones. It is found that the fracture strength of all the samples is between 1918 MPa and 1955 MPa, showing no obvious variation dependence of the annealing states. This indicates that the local atomic structure is not changed by the annealing obviously, which is consistent with the results by XRD and DSC. There rises a question: why the reduction in atomic mobility, corresponding to the increase in microhardness, does not have much impact on the fracture strength?

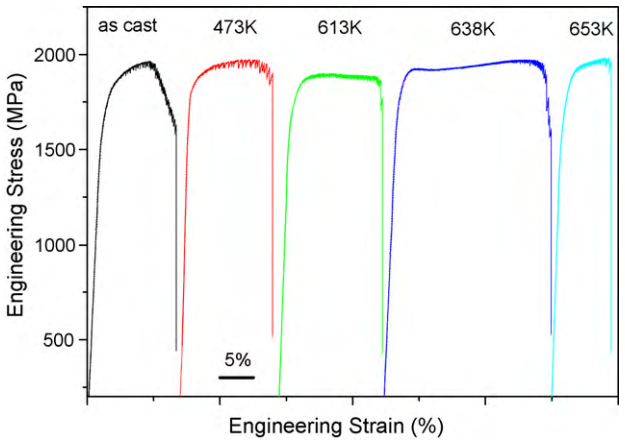

Fig. 7. The room temperature compression stress–strain curves of the 2 mm $Zr_{63.78}Cu_{14.72}Ni_{10}Al_{10}Nb_{1.5}$ BMG rods at a initial strain rate of 5×10^{-5} s^{-1} at different annealing temperature.

The average plastic strains for the as-cast and annealed samples below T_g remains almost the same in spite of the dramatic variation in FV content, and the average values are $10.4 \pm 1.6\%$, $10.4 \pm 2.5\%$, $10.2 \pm 3.5\%$ and $10.2 \pm 5.8\%$ for the as-cast samples and the samples annealed at 473 K, 613 K and 638 K, respectively. These results are quite different from those previous results of embrittlement after annealing the BMGs below T_g due to the structural relaxation and FV annihilation. The morphology of the fracture and side surfaces of the partial broken rods is shown in Fig. 8. The multiple shear bands and the severe intersection of shear bands exist on the side surfaces of all the rods. The fracture morphology displays a great deal of plastic characters, for example, deep vein patterns and deep ridges with short spacing of ~8 μm. All these evidences indicate that the BMGs exhibit the good plasticity. Although their volume dilates by 0.101%, the samples annealed just above T_g (653 K) exhibit a relatively lower average plastic strain of $8.2 \pm 0.4\%$. The results further show that there is intrinsic difference between the expansion caused by the glass transition and the relatively loose structure introduced by the excess FV. The former does not favor the plastic deformation, while the latter does.

What intrinsic features cause the unusual plastic deformability in $Zr_{63.78}Cu_{14.72}Ni_{10}Al_{10}Nb_{1.5}$ BMGs in spite of the annealing states and the FV content? In the intrinsic view, the deformation in BMGs is related to a stress-driven structure disordering process through the collective motion of several tens of atoms as proposed in the framework of the shear transformation zone (STZ) theory, accompanying the dilatation in volume and excess FV formation [30–32]. The STZ operations cause the local evolution of structural order and then cause the strain softening and shear localization or shear band formation. Comparing with the crystalline counterparts, BMGs contain a certain amount of excess FV. The amount and distribution of FV may have obvious impact in STZ operation and shear bands initiation. More shear bands formation and the interaction and impediment among these shear bands favor the macro-plastic deformation in BMGs. Falk and Torre et al. find that the apparent activation volume is a key parameter to operate a STZ [33–35]. Torre and co-workers have experimentally measured the apparent activation volume of a Zr-based BMG by conducting the variable strain rate experiments at different temperature [33,34]. From their results, it is concluded that the apparent activation volume is above 3.6 nm^3 at the intermediate temperature, however, about 0.1–0.15 nm^3 at the lower or higher temperature, which is consistent with the results by other researchers [36]. Smaller apparent activation volume facilitates an easier collective atoms motion and STZ operation and then favors more shear bands initiation, therefore, results in the larger plastic deformation. Also the results explain that the poor plasticity at room temperature is due to the large apparent activation volume and the difficulty in STZ operation and shear bands initiation. Then we examine the influence of minor Nb addition on the structure changes of ZrCuNiAl BMGs.

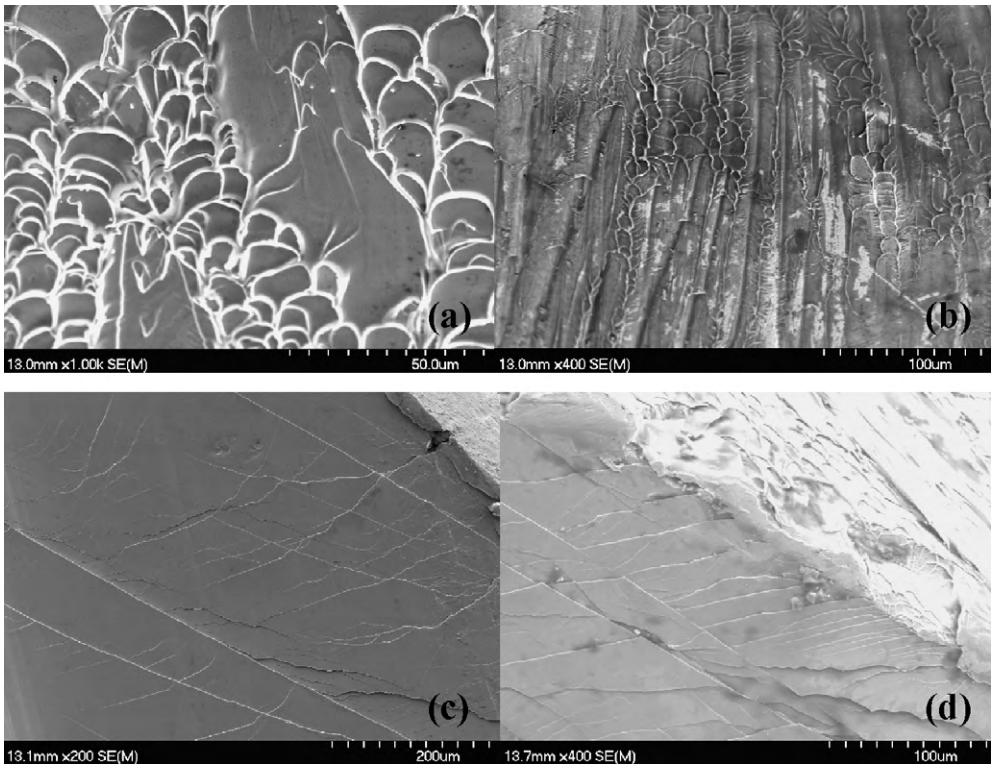

Fig. 8. The SEM micrographs of the fracture and side surfaces of the partial broken rods for the $Zr_{63.78}Cu_{14.72}Ni_{10}Al_{10}Nb_{1.5}$ BMGs annealed at 473 K (a and c) and 613 K (b and d).

The values of heat of mixing for Nb–Zr, Nb–Cu, Nb–Al and Nb–Ni atom pairs are 4, 3, −18 and −32 kJ/mol, respectively, while that for Zr–Cu, Zr–Al and Zr–Ni atom pairs are −23, −44and −51 kJ/mol, respectively [37]. These indicate that Nb is more easily to bond with Cu, Al, and Ni than Zr and tends to substitute Zr in the ZrCuNiAlNb system. On the other hand, the atomic radius of Nb (0.143 nm) is relatively smaller than that of Zr (0.162 nm) [38], so this substitute of Zr with Nb results in more excess FV [28]. Then, it is reasonable to speculate that the increased FV caused by the atomic size discrepancy can be located in a small atomic cluster and do survive the structural relaxation induced by annealing, while the FV caused by quenching can be depleted by the atomic diffusion at the external heating. The relatively smaller clusters containing the additional FV may act as potential sites to operate STZ and then initiate shear bands, indicating that the minor Nb addition can effectively reduce the apparent activation volume and consequently favor the plastic deformation.

We then examine the fracture strength again. The failure of BMGs is generally dominated by various parameters, for example, the microstructure, the atomic binding energy, the elastic constants, T_g, etc., along with the atomic mobility. Under the conditions of these experiments, annealing only provokes the short-range atomic diffusion and exerts no appreciable change in the structure and atomic bonding of the BMGs. The failure of BMGs essentially involves the breakage of the small atomic clusters, which is not changed by the structural relaxation after annealing. So the ultimate fracture strength does not change obviously in spite of the relatively higher flow stress caused by the more difficult atomic mobility after experiencing an annealing history.

4. Conclusions

In order to study the structural stability and the mechanical properties of BMGs experienced the structural relaxation, the $Zr_{63.78}Cu_{14.72}Ni_{10}Al_{10}Nb_{1.5}$ BMG rods were subjected to dilatometric measurements, microhardness tests and uniaxial compression. Based on the experimental results and the detailed analysis, the following conclusions can be drawn:

(1) The $Zr_{63.78}Cu_{14.72}Ni_{10}Al_{10}Nb_{1.5}$ BMGs sustain good structural stability and unusual plastic deformability after isothermal relaxation at 473 K, 613 K, 638 K and 653 K for 3600 s.
(2) There are two visible structural relaxation processes at 466 K and 599 K, respectively defined by the constant-heating dilatometric measurements. More than 70% of the REFV occurs at the 2nd main relaxation temperature (599 K).
(3) The microhardness of the BMGs increases with increasing the structural relaxation temperature and the depletion of FV of BMGs, while the fracture strength does not change distinguishingly.
(4) Although there is the phenomenological similarity, there is intrinsic difference between the expansion caused by the glass transition and the relatively loose structure introduced by the excess FV. The former does not favor the plastic deformation in BMGs, while the latter does.
(5) The $Zr_{63.78}Cu_{14.72}Ni_{10}Al_{10}Nb_{1.5}$ BMGs annealed below T_g attain the same plasticity just as the as-cast ones. This unusual plastic deformability is ascribed to the reduction in the apparent activation volume with the minor Nb addition.

Acknowledgments

This research was supported by Shenzhen Science and Technology Research Grant (Grant No. CBX200903090012A) and the Open Project Program of Shenzhen Key Laboratory of Special Functional Materials (Grant No. T0907). The authors thank G.Q. Luo and W.C. Lin for their help in the experiments.

References

[1] A. Inoue, Acta Mater. 48 (2000) 279–306.
[2] M.F. Ashby, A.L. Greer, Scripta Mater. 54 (2006) 321–326.
[3] L. Zhang, Y.-Q. Cheng, A.-J. Cao, et al., Acta Mater. 57 (2009) 1154–1164.
[4] C.C. Hays, C.P. Kim, W.L. Johnson, Mater. Sci. Eng. A 304–306 (2001) 650–655.
[5] P. Murali, U. Ramamurty, Acta Mater. 53 (2005) 1467–1478.
[6] F.F. Wu, Z.F. Zhang, S.X. Mao, et al., Phys. Rev. B 75 (2007) 134201.
[7] A.L. Greer, Science 267 (1995) 1947–1953.
[8] W.H. Wang, C. Dong, C.H. Shek, Mater. Sci. Eng. R44 (2004) 45–89.
[9] E.S. Park, J.S. Kyeong, D.H. Kim, Scripta Mater. 57 (2007) 49–52.
[10] C. Fan, C.F. Li, A. Inoue, J. Non-Cryst. Solids 270 (2000) 28–33.
[11] U. Kuhn, N. Mattern, A. Gebert, et al., J. Appl. Phys. 98 (2005) 054307.
[12] Z.W. Zhu, S.J. Zheng, H.F. Zhang, et al., J. Mater. Res. 23 (2008) 941–948.
[13] C. Fan, T.W. Dongchun Qiao, Wilson, et al., Mater. Sci. Eng. A 431 (2006) 158–165.
[14] D.G. Pan, H.F. Zhang, A.M. Wang, et al., Appl. Phys. Lett. 89 (2006) 261904.
[15] W. Loser, J. Das, A. Guth, et al., Intermetallics 12 (2004) 1153–1158.
[16] K. Mondal, T. Ohkubo, T. Toyama, et al., Acta Mater. 56 (2008) 5329–5339.
[17] J. Pan, L. Liu, K.C. Chen, Scripta Mater. 60 (2009) 822–825.
[18] K. Hajlaoui, B. Doisneau, A.R. Yavari, et al., Mater. Sci. Eng. A 449–451 (2007) 105–110.
[19] S.-W. Lee, M.-Y. Huh, E. Fleury, et al., Acta Mater. 54 (2006) 349–355.
[20] Y.H. Liu, G. Wang, R.J. Wang, et al., Science 315 (2007) 1385–1388.
[21] L.Y. Chen, Z.D. Fu, G.Q. Zhang, et al., Phys. Rev. Lett. 100 (2008) 075501.
[22] L.Y. Chen, A.D. Setyawan, H. Kato, et al., Scripta Mater. 59 (2008) 75–78.
[23] X. Hu, S.C. Ng, Y.P. Feng, et al., Phys. Rev. B 64 (2001) 172201.
[24] V.H. Hammond, M.D. Houtz, J.M. O'Reilly, J. Non-Cryst. Solids 325 (2003) 179–186.
[25] A. Slipenyuk, J. Eckert, Scripta Mater. 50 (2004) 39–44.
[26] W. Dmowski, C. Fan, M.L. Morrison, et al., Mater. Sci. Eng. A 471 (2007) 125–129.
[27] K.S. Lee, J.-H. Lee, J. Eckert, Intermetallics 17 (2009) 222–226.
[28] S.H. Xie, X.R. Zeng, H.X. Qian, J. Alloys Compd. 480 (2009) L37–L40.
[29] H. Kato, H.-S. Chen, A. Inoue, Scripta Mater. 58 (2008) 1106–1109.
[30] Q. Chen, L. Liu, K.C. Chan, J. Alloys Compd. 467 (2009) 208–212.
[31] B.P. Kanungo, S.C. Glade, P. Asoka-Kumar, et al., Intermetallics 12 (2004) 1073–1080.
[32] M.L. Falk, Phys. Rev. B 60 (1999) 7062.
[33] A. Dubach, F.H. Dalla Torre, J.F. Loffler, Acta Mater. 57 (2009) 881–892.
[34] F.H. Dalla Torre, A. Dubach, E. Marco, M.E. Siegrist, et al., Appl. Phys. Lett. 89 (2006) 091918.
[35] R. Raghavan, P. Murali, U. Ramamurty, Acta Mater. 57 (2009) 3332–3340.
[36] M. Bletry, P. Guyot, J.J. Blandin, et al., Acta Mater. 54 (2006) 1257–1263.
[37] T. Akira, A. Inoue, Mater. Trans. 46 (2005) 2729–2817.
[38] S. Nagasaki, M. Hirabayashi (Eds.), Binary Alloy Phase Diagrams, 1st ed., Metallurgical Industry Press, Beijing, 2004, A.S. Liu (transl.).